



UNIVERSIDADE ESTADUAL DE CAMPINAS  
SISTEMA DE BIBLIOTECAS DA UNICAMP  
REPOSITÓRIO DA PRODUÇÃO CIENTÍFICA E INTELLECTUAL DA UNICAMP

**Versão do arquivo anexado / Version of attached file:**

Versão do Editor / Published Version

**Mais informações no site da editora / Further information on publisher's website:**

<https://www.sciencedirect.com/science/article/pii/S0008622314006666>

**DOI: 10.1016/j.carbon.2014.07.028**

**Direitos autorais / Publisher's copyright statement:**

©2014 by Elsevier. All rights reserved.

DIRETORIA DE TRATAMENTO DA INFORMAÇÃO

Cidade Universitária Zeferino Vaz Barão Geraldo

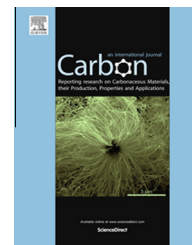
CEP 13083-970 – Campinas SP

Fone: (19) 3521-6493

<http://www.repositorio.unicamp.br>

Available at [www.sciencedirect.com](http://www.sciencedirect.com)

ScienceDirect

journal homepage: [www.elsevier.com/locate/carbon](http://www.elsevier.com/locate/carbon)

# Multifunctional and environmentally friendly nanocomposites between natural rubber and graphene or graphene oxide

Carolina F. Matos <sup>a</sup>, Fernando Galembeck <sup>b</sup>, Aldo J.G. Zarbin <sup>a,\*</sup>

<sup>a</sup> Departamento de Química, Universidade Federal do Paraná (UFPR), Curitiba, PR, Brazil

<sup>b</sup> Instituto de Química, Universidade Estadual de Campinas (UNICAMP), Campinas, SP, Brazil

## ARTICLE INFO

### Article history:

Received 22 April 2014

Accepted 10 July 2014

Available online 18 July 2014

## ABSTRACT

This work describes a green route to multifunctional nanocomposite materials composed of natural rubber (NR) latex and graphene (rGO) or graphene oxide (GO). Aqueous solutions with different concentrations of GO and rGO (prepared with the surfactant cetyltrimethylammonium bromide – CTAB) were mixed with natural rubber latex under magnetic stirring followed by sonication. The slurries obtained after casting were dried in an oven in air at 70 °C for 24 h. The nanocomposites were characterized by TEM and SEM, AFM and KFM. The thermal, electrical and mechanical properties were evaluated using TGA, resistivity measurements (four-point) and DMA. Swelling tests were performed using three solvents with different polarities: xylene, isopropanol and water. The inclusion of filler networks in the polymeric matrices provided significant improvements in the electrical, chemical and mechanical properties, in comparison to the unfilled polymer. In addition, the nanocomposites proved to be biodegradable.

© 2014 Elsevier Ltd. All rights reserved.

## 1. Introduction

To minimize the environmental impacts caused by polymers, several alternatives have been proposed. One alternative is the use of biodegradable materials, which can be degraded by microorganisms. However, the use of these materials at large scales becomes complicated due to the poor mechanical, electrical and thermal properties of some biodegradable polymers. Therefore, the need for replacements for such materials is clear, and a very recent alternative is the use of nanocomposites, in which different polymers are mixed with different fillers as layered materials, such as silicates and clay minerals [1], and allotropes of carbon, such as amorphous carbon [2], carbon fiber [3], carbon nanotubes [4], graphene

[5] and graphene oxide [6]. The so-called nano-biocomposites are obtained by adding nanoparticles to polymers, which results in very promising materials because they have improved properties and preserve the biodegradable polymeric material [7,8].

A biopolymer with unique properties that is ideal for the synthesis of this type of material is natural rubber (NR). Composed mainly of *cis*-poly(1,4-isoprene), natural rubber is extracted in the form of latex from the *Hevea brasiliensis* tree, popularly known as the rubber tree, which is native to the Amazon Forest [9]. Natural rubber is the most important biosynthesized rubber and shows excellent physical and chemical properties, such as elasticity, flexibility and antiviral permeation. Additionally, NR is easily moldable and highly

\* Corresponding author.

E-mail address: [aldozarbin@ufpr.br](mailto:aldozarbin@ufpr.br) (A.J.G. Zarbin).

<http://dx.doi.org/10.1016/j.carbon.2014.07.028>

0008-6223/© 2014 Elsevier Ltd. All rights reserved.

biodegradable. A practical example of the importance of natural rubber is in the manufacturing of tires for trucks, buses and airplanes, which are not made using synthetic rubber only.

Several studies involving the preparation of different NR-based nanocomposites, aiming materials that have improved properties and further expand the potential applicability of NR, have been reported. Graphene and its relatives (graphene oxide, reduced graphene oxide, graphene nanoribbons, among others) are promising candidates as fillers in NR-based nanocomposites due to the range of unique properties of these materials, such as high specific surface area, high thermal and electrical conductivity, mechanical strength and flexibility, among many others. Thus, the incorporation of graphene-based species has been shown to be useful, particularly in improving the mechanical, thermal and electrical properties of NR, transforming the NR in a multifunctional material [10,11].

There are different techniques used to prepare multifunctional nanocomposites of NR and graphene species [12,13]. A relatively new approach to incorporate carbon nanostructures in a polymeric matrix is based on the use of the so-called *latex technology*, in which the filler is directly mixed to the aqueous colloidal dispersion of the polymer (latex) [14]. This process is fast (because it basically consists of a simple mixture of two aqueous components), versatile, reliable and reproducible. Also, as the solvent used in all steps is water, the process is safe, environmentally friendly and inexpensive [15]. Studies involving graphene/NR generally employ *in situ* reduction of the graphene oxide (using reducing agents such as  $N_2H_4$  and  $NaBH_4$ ) inside the latex matrix, followed by coagulation and, generally, press-curing [16,17]. However, there are no reports comparing the properties of different NR-based nanocomposites prepared with either graphene oxide (GO) or reduced graphene oxide (rGO) as fillers. It is expected that due to different structural and chemical properties of each one of these graphene-like structures (such as electrical conductivity, water solubility, presence of oxygenated functional groups, among others), the different fillers should interact in a different way with the polymeric latex, resulting in materials with different properties.

In this paper we propose a simple and environmentally friendly approach for the synthesis of NR/graphene and NR/graphene oxide multifunctional composites materials, based on the latex technology. The obtained composites were characterized by different techniques, and some properties were evaluated and comparatively discussed.

## 2. Experimental

### 2.1. Materials

Natural rubber latex (NR,  $T_g = -62 \pm 1$  °C,  $\zeta = -80 \pm 4$  mV and with a total solid content of  $62.4 \pm 0.1\%$ ) was supplied by Talismã (Mirassol, Brazil). Graphene oxide (GO) and reduced graphene oxide (rGO) were obtained through a modified Hummers method [18]. The GO was reduced using sodium borohydride –  $NaBH_4$  (Merck). All the water used was deionized using a Milli-Q system. The surfactant cetyltrimethylammonium bromide – CTAB (Sigma-Aldrich) was used as received.

### 2.2. Preparation of the nanocomposites

For the synthesis of natural rubber/graphene oxide (NRGO) nanocomposites, appropriate volumes of a dispersion containing  $1 \text{ mg mL}^{-1}$  of GO were added to the natural rubber latex (Table 1) and homogenized for 30 min using magnetic stirring. Then, the mixture was sonicated for another 10 min to remove the bubbles formed during the stirring process. Finally, the mixture was added to a mold and placed in an oven at 70 °C until the material was completely dry.

For the synthesis of the natural rubber/reduced graphene oxide composites (NRrGO), the rGO was initially dispersed in 20 mL of an aqueous CTAB solution (0.5 wt/v) for 2 h in an ultrasonic bath. The next step involved mixing the dispersions of rGO with latex using magnetic stirring (2000 rpm) for 30 min and sonication for another 10 min. Finally, in the same way as the composites prepared with GO, the mixtures were placed in molds and oven dried (70 °C). Several composite samples were prepared that contained different amounts of filler, i.e., from 0.01 to 10 wt% dried NR. The fraction of filler in the composites was calculated based on the weight of dry polymer. For example, to prepare the composite 1NRrGO, starting from 2 g of latex, we consider 1.24 g of dry rubber (considering solids content of 62.4%). So, the amount of filler used to prepare this composite corresponds to 1 wt% of 1.24 g, therefore  $\sim 12$  mg of rGO. The amounts of nanostructures and latex used to prepare all the composites are specified in Table 1.

The samples will be referred to by the following designations: NR for natural rubber without nanostructures (used as the control sample), NRrGO for the natural rubber composites prepared with reduced graphene oxide and CTAB, and NRGO for the natural rubber composites prepared with graphene oxide. The number that precedes the acronyms represent the percentages of nanostructures by weight (based on dry polymer) added to the composite.

### 2.3. Characterization

Transmission electron microscopy (TEM) images were acquired using a Carl Zeiss Libra 120 kV transmission electron microscope equipped with an omega filter and operating at 80 kV. Ultrathin cuts of the transverse sections of the composites 2NRGO and 2NRrGO were obtained using an ultra-cryomicrotome (LAICA) with diamond knives (Drukker) at  $-140$  °C. The thin cuts were collected directly on copper grids and dried under ambient conditions. Elemental maps of 20 times diluted 1NRrGO composite (i.e., 1 mL of the freshly prepared mixtures of the composite were diluted with another 19 mL of water) were acquired by imaging inelastically scattered electrons using electron spectroscopy imaging (ESI). The images were recorded using a CCD camera and an iTEM Universal TEM Imaging Platform. Characteristic energy losses for interaction of electrons with C (303 eV) and N (410 eV) were selected using an energy slit of 10 eV.

Field electron gun scanning electron microscopy data of fractured surfaces of the 2NRGO and 2NRrGO nanocomposites in liquid  $N_2$  were analyzed using a Tescan equipment operated at 15 kV. The samples were metalized with chromium.

**Table 1 – Amounts of reagents used for the preparation of the different nanocomposites between natural rubber latex and graphene oxide or reduced graphene oxide.**

Sample	Filler/NR ratio (w/w)	Latex (g)	rGO (mg) or GO (mL)
NR	–	2	–
0.1NRrGO	0.1	2.045	1.341
0.5NRrGO	0.5	2.0452	6.321
1NRrGO	1.0	2.0987	12.51
2NRrGO	2.0	2.0767	25.01
5NRrGO	5.0	2.1004	48.97
10 NRrGO	10.0	2.1946	95.98
0.1NRGO	0.1	2.089	1.40
0.5NRGO	0.5	2.1009	6.40
1 NRGO	1.0	2.0967	13.0
2 NRGO	2.0	2.0786	25.0
5 NRGO	5.0	1.2562	38.0
10 NRGO	10.0	0.7781	47.0

Atomic force microscopy (AFM) images were obtained in non-contact mode using an SPM 9700 (Shimadzu) microscope. A piece (1 × 1 mm) of the 2NRGO sample was used to evaluate the face that was fractured in liquid N<sub>2</sub> and the surface of the film roughed by the cryo-microtome. The phase angle  $\theta = -90^\circ$  was chosen because the brighter domains in the images are more dissipative than the darker domains.

Kelvin Force Microscopy (KFM) images were obtained from the 1NRrGO and 1NRGO samples before drying and diluting 20 times. The dispersion droplets were allowed to dry on top of freshly cleaved mica surfaces. The samples were dried at 30 °C prior to mounting on the scanning probe microscope sample holder. Electrostatic patterns in the submicrometer range were obtained using electric potential scanning probe microscopy (KFM) with a Shimadzu SPM 9700 instrument. The KFM technique used the standard noncontact AFM setup, but the sample was scanned with Pt-coated Si tips with a 20 nm nominal radius.

Thermogravimetric analyses (TGA) were performed on a SDT Q600 (TA Instruments) under an atmosphere of synthetic air (White Martins, 100 mL/min) from room temperature to 1000 °C at a heating rate of 5 °C min<sup>-1</sup>.

The resistivity values of the samples were measured directly from the composites (squares with 1 cm sides and 0.5 mm thickness) using the four-point technique using a Jandel Universal probe. The distance between the points was fixed at 1.0 mm.

Dynamical mechanical tests were performed on a Netzsch model 242 dynamic mechanical analyzer using a frequency of 1 Hz from -120 to 30 °C, with a tensile mode at an amplitude of 50 μm and a heating rate of 3 °C min<sup>-1</sup>, in an atmosphere of nitrogen at a flow rate of 50 mL min<sup>-1</sup>. The tests were performed according to ASTM D5026-01. The storage modulus ( $E'$ ), damping ( $\tan \delta$ ) and loss factor ( $E''$ ) were evaluated.

For the swelling measurements, three solvents were used with different polarities: xylene, isopropyl alcohol and water. Square pieces (1 cm wide and ~0.5 mm thick) of the samples were cut, and the thickness of each sample was measured using a pachymeter. The initial weight was determined, and the samples were immersed in approximately 50 mL of each

solvent. The samples were removed from the flasks after 20, 40 and 60 min. The adhering solvent was blotted off the surface, and the samples were quickly weighed. All dimensions of the samples were also measured, and then, they were immediately returned to the flasks until the end of the experiment (60 min).

The biodegradability tests were performed using a methodology described by ASTM G160-03. The soil used was prepared from a mixture of equal parts of sand, soil and horse manure. The soil was aged for a period of 3 months, and the factors that affect the results, such as humidity and pH, were controlled. The biodegradabilities of the pure natural rubber and 2NRrGO and 2NRGO nanocomposites were evaluated over a period of one year at intervals of 3, 6 and 12 months. The samples were cut to 1 × 1 cm and weighed on an analytical balance. The specimens were placed in small screen packages which were closed with nylon threads. The materials were buried (at a depth of 10–15 cm) in a plastic container containing standard soil. After periods of 3, 6 and 12 months the samples were removed from soil, washed, dried, weighed and analyzed by FTIR-ATR and Raman spectroscopy. The values of the degraded mass were obtained by the difference between the initial mass and the mass determined after the period of degradation. Samples without any contact with the soil were used as control.

The Raman spectra were obtained on a Renishaw Raman Imaging Microscope Equipment System 3000 coupled to an optical microscope. The laser used was a He-Ne laser (emitting at 632.8 nm).

The samples were analyzed on a Vertex-70 (Bruker) in attenuated total reflectance (ATR) mode using an ATR accessory (Pike Technologies). Scans were performed in the region 600–4000 cm<sup>-1</sup>.

### 3. Results and discussion

TEM images of the dry diluted 1NRGO (Fig. 1a) and 1NRrGO (Fig. 1d and g) dispersions are shown in Fig. 1. In these images (collected from the diluted mixture of each component before the latex coalescence), we can see that the graphene sheets

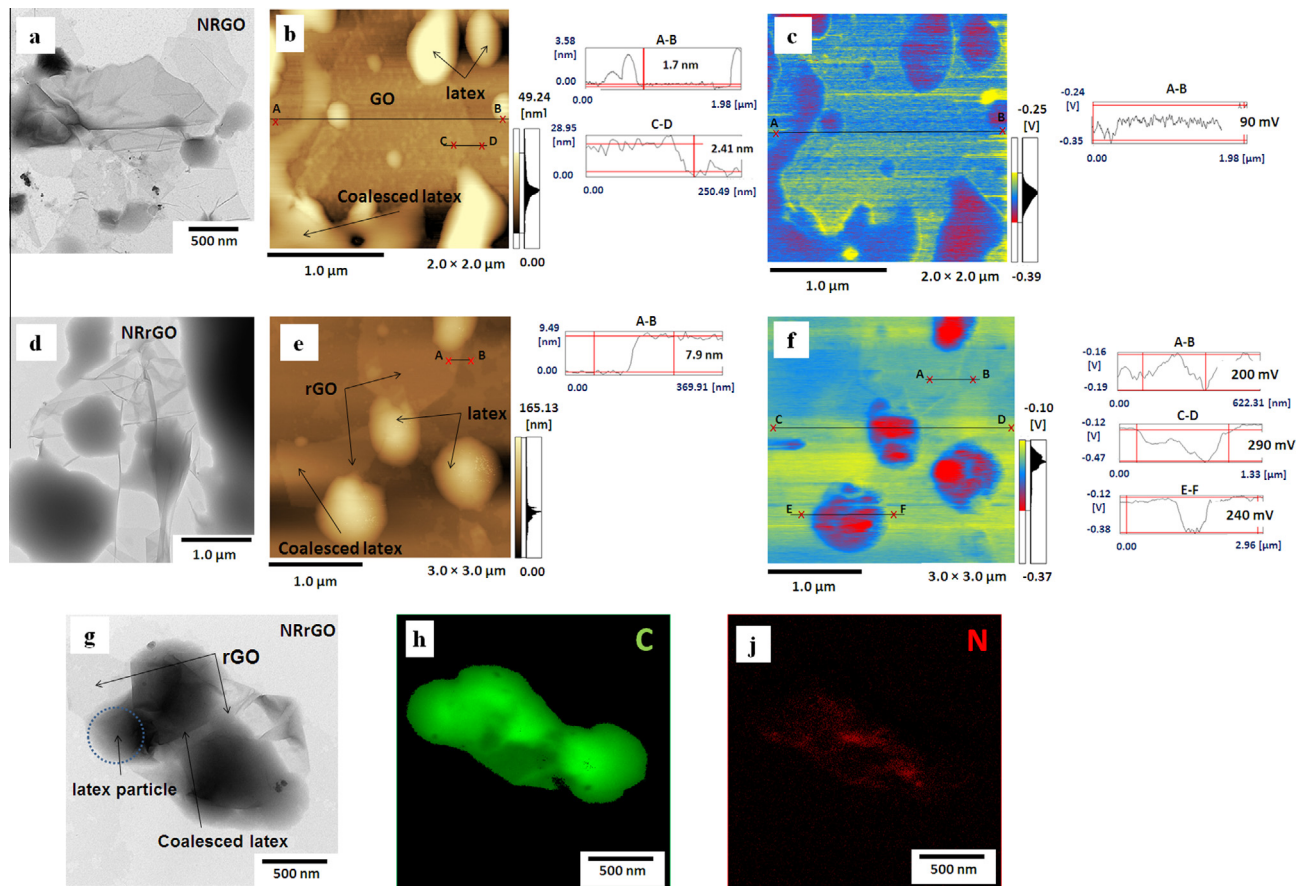


**Fig. 1** – TEM bright-field images (a, d, g), AFM images (b, e), KFM images (c, f) of dry diluted dispersions 1NRGO (a–c) and 1NRrGO (d–f); and TEM elemental maps of: (h) carbon and (j) nitrogen of the composite 1NRrGO. (A colour version of this figure can be viewed online.)

adhere to the latex particles, many of which are in a coalescent process. The same is observed in the AFM topographical images (Fig. 1b and e). Evaluating the profile of GO and rGO, we observe thicknesses of  $\sim 1.7$  and  $\sim 7.9$  nm, respectively, for these two materials. The first corresponds to a GO bilayer while the later shows that for rGO a multilayer [19]. Both KFM images show that latex is not a homogeneous material in terms of the distribution of the electric potential due to the accumulation of negative charges inside the particles. At the interface between the particles, the potential is more positive [20]. KFM images of the 1NRGO composite (Fig. 1c) shows both components are negatively charged, and the potential difference on the surface reaches 90 mV (profile A–B Fig. 1c); the negative potential, however, is not greater than  $-250$  mV (scale side of the image). The edge region of the GO features accumulates positive charges that are ions from the latex serum, such as phospholipids (which are positively charged) and cations (as magnesium, potassium, copper, and ammonium), which can interact with the oxygenated groups present on the GO surface. Fig. 1f shows the surface potential microscopy image of the same region of the 1NRrGO composite evaluated in Fig. 1e. Comparison with the sample containing GO shows significant differences in the charge distribution, reaching a  $\Delta V$  value of 290 mV on the surface (profile C–D Fig. 1f), with a maximum potential of  $-100$  mV

(150 mV higher than the 1NRGO sample). In some regions of the 1NRrGO composite, there is a higher density of positive charges due to the coalescence of the latex particles. We can also observe a nonhomogeneous distribution of these positive charges on the sheets of the rGO. This behavior indicates that CTAB, which is a cationic surfactant, remains mainly at the edges of the rGO sheet, and in the coalesced rubber, it plays an important role in the interaction of the rGO and the matrix. This result is confirmed by elemental mapping. The bright-field image shown in Fig. 1g shows a sheet of rGO wrapping around some latex particles as well as a region where the latex begins to coalesce. A carbon map of this same region (Fig. 1h) shows the region containing the polymer and the rGO in green. In the elemental map of nitrogen (Fig. 1j in red), we observed a higher concentration of this element (from CTAB) in the same coalesced latex and over the rGO.

Similar results were described by Kim et al. [21] that demonstrated by zeta potential measurements an increase in the potential of pure styrene-butadiene rubber latex (SBR) latex caused by the addition of multi-layer graphene/CTAB dispersion. The authors stated that CTAB-stabilized multi layered graphene is more effectively dispersed in the SBR matrix due to electrostatic attraction between the filler and the negative-charged SBR colloidal particles.

Comparing the composites prepared with the two different fillers (GO and rGO) it is clear that the total potential on the surfaces of both composites are negative, due to the anionic nature of the latex, which is the major component in the final material. However, due to the presence of the CTAB adhered in the rGO sheets in the NRrGO composite, a significantly higher difference of potential is detected in this material, resulting in a higher electrostatic attraction between the components. Such differences in the distribution topology and charge on the composite can have important consequences for the mechanical properties of the film and the properties of the surface (for example, the adhesiveness).

After the coalescence, the morphology of the consolidated composites was evaluated using scanning and transmission electron microscopies (SEM and TEM) and atomic force microscopy (AFM) of fracture or cut surfaces of 2NRrGO and 2NRGO solid samples. In the SEM images (Fig. 2), we observe homogeneous surfaces for both systems. Aggregates were rarely found on the analyzed surfaces (not even fragments of graphite or graphite oxide remaining from the rGO synthesis), showing the efficiency of the dispersion of the film.

Fig. 3 shows the AFM images of the cross-section of the samples 2NRrGO and 2NRGO, in topographical and phase contrast modes. It is possible to observe, in addition to the smooth topography, differences in the viscoelastic properties of the matrix and the particles embedded in the polymeric matrix in the phase images (Fig. 3b and d), where the matrix is softer (bright regions) than the particles (darker). It is believed that the population of particles is composed mainly of crystals of  $\text{CaSO}_4$ , which are naturally present in natural rubber latex [22], and possibly small aggregates of rGO and GO. This difference is better viewed in the image of the NRrGO composite.

The 2NRrGO and 2NRGO samples were also analyzed by TEM. Fig. 4 shows representative micrographs from thin cuts. The dark lines are the cross-sections of single or multiple sheet layers (1–10-nm thick) non-uniformly distributed, but well incorporated into the rubber matrix. In these micrographs, it is possible to observe some thicker multilayer tactoids. This feature was also observed by Pottes et al. [23] in NRrGO composites prepared using latex coagulation and by Valadares et al. [24] in composites with natural rubber–montmorillonite prepared by casting.

Fig. 5a shows the storage modulus curves obtained using DMA for NR and rGO and GO nanocomposites. At temperatures above the  $T_g$ , the storage modulus of the composite materials increases with increasing in the filler content, especially at room temperature. The mechanical properties of the polymers are improved due to the combination of the high surface area, high rubber-particle adhesion and high modulus of the incorporated nanostructures, resulting in a linear increase in the storage modulus of the nanocomposites according to the amount of filler added. Comparing the storage modulus at 20 °C of the samples containing 2 wt% of filler with neat NR (Fig. 5b), the modulus increased by a factor of 1.7 and 3.3 for the rGO and GO composites, respectively. Improvements on the same order have been described in samples of milled NRrGO nanocomposites [23]. The improved performance of the GO-based sample may be associated to the better homogeneity of these films and probably also to higher particle–matrix adhesion.

Regarding the loss modulus (Supporting information, Fig. S1), there was a significant increase in this parameter as a function of the addition of the nanostructures, which is similar to the storage modulus. This increase, which is

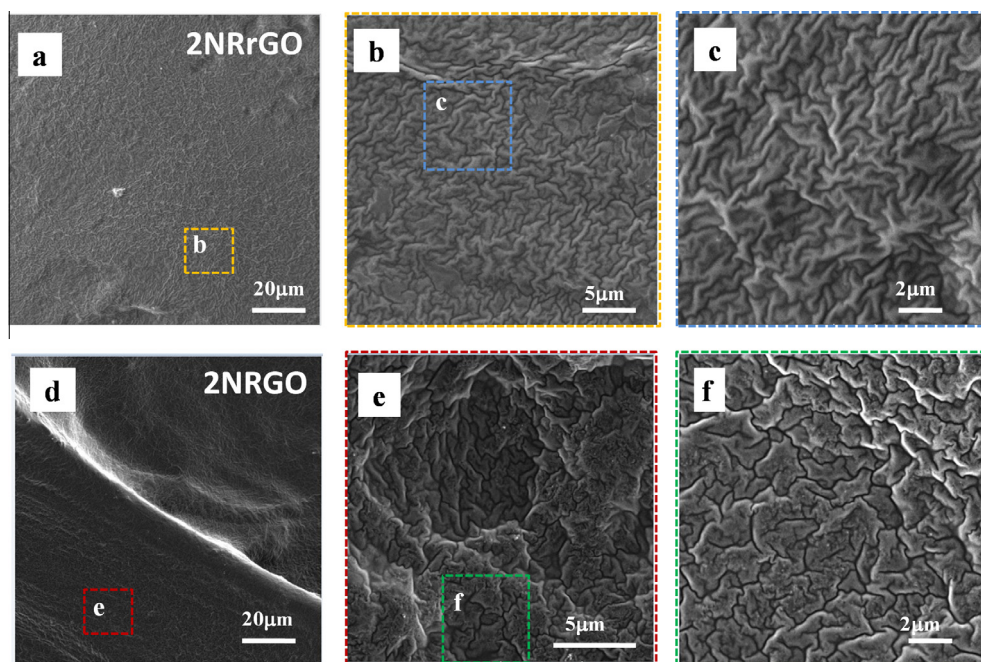
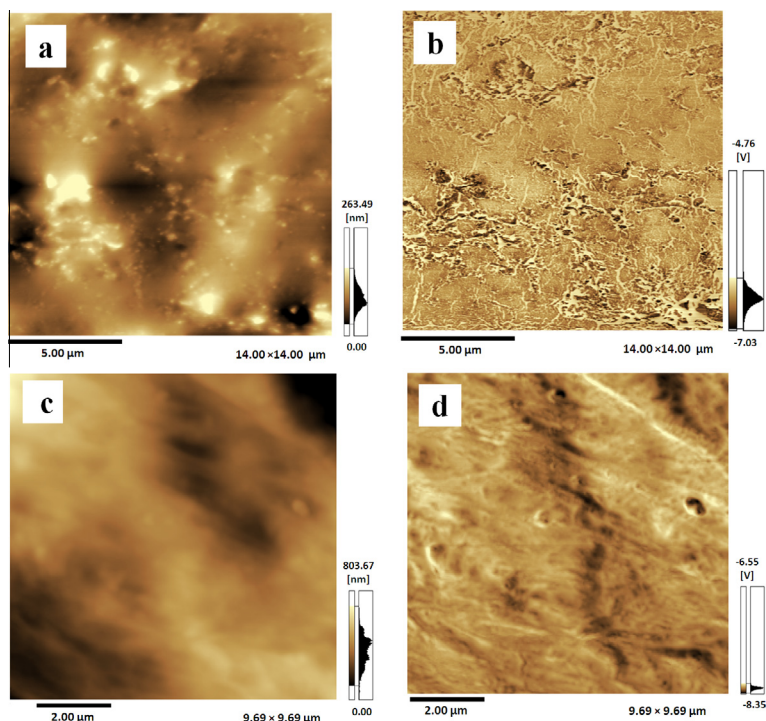


Fig. 2 – (a–c) SEM images of a 2NRrGO nanocomposite: (a) panoramic image of the cross section; (b) details of the region marked in yellow in the image (a); (c) detail of the region marked in blue in the image (b); (d–f) SEM images of a 2NRGO composite: (d) panoramic image of the cross section; (e) details of the region marked in red in the image (d); (f) detail of the region marked in green in (e). (A colour version of this figure can be viewed online.)



**Fig. 3 – Topographical (a, c) and phase contrast (b, d) AFM images of the transverse cross-section the 2NRrGO (a, b) and 2NRGO (c, d) nanocomposites. (A colour version of this figure can be viewed online.)**

associated with an increase in the width of the peak  $\tan \delta \times T$  (Fig. 6) for a certain relaxation, indicates that the material exhibits a broader range of frequencies that can be absorbed, i.e., this material has a higher potential than the neat NR for acoustic insulation [25], ranging for example from acoustic insulation for airplanes to use in construction.

The variations in  $\tan \delta$  as a function of temperature for all materials studied are shown in Fig. 6. The height of the  $\tan \delta$  peak, which corresponds to the glass transition temperature ( $T_g$ ) of the elastomer, is reduced and enlarged after the introduction of the fillers. This behavior can be explained in terms of a decrease in the fraction of polymer in the composite. At low temperatures, the mechanical energy is dissipated by the motion of polymer chains because the small, solid particles embedded in the matrix are not efficient at absorbing energy. Also, in the nanocomposite, the extent of polymer chain motion restriction by interspersed particles varies widely depending on the size of the contacting chain segment. At higher temperatures (the rubber state), hysteresis tends to increase due to the presence of fillers [26]. This result may also be associated with the fact that the network formed by these nanostructures can be broken, causing additional energy dissipation and, therefore, a rubber hysteresis in this region [27].

Another effect observed in the  $\tan \delta$  curves is the appearance of a second region (such as a shoulder on the main peak – see Supporting information, Fig. S2) indicating the presence of two phases containing different  $T_g$ , one at lower and one at higher temperatures than the pure polymer (Table S1 shows the  $T_g$  values). This result may be related to the fact that some particles restrict the flow of some polymer chains, resulting in an incomplete relaxation of the terminal regions

and partial crosslinking in the polymer, which is not filled, resulting in the appearance of peaks in  $\tan \delta$  higher than the main peak. That is, the polymers that are interacting directly with surfaces of the filler are immobilized (diffusion chain relaxation/reptation) and have different characteristics than the other fraction of the polymer, which is not directly associated with the nanostructures [28]. This result is an evidence of the efficient interaction between the graphene or graphene oxide and the natural rubber matrix. The occurrence of lower-temperature  $T_g$  peak should be explained by the following: polymer chain-particle interaction is expected to cause polymer partition, according to data from polymer adsorption from solutions. The larger chains are preferentially bound to particles, creating domains enriched in shorter chains and/or plasticizing small molecules, like phospholipids. Lower-temperature  $T_g$  corresponds to material in these domains.

The effect of the presence of the nanostructures on the thermal stability of natural rubber was evaluated using thermogravimetric analysis (TGA), as shown in Fig. 7.

Neat NR, when degraded under an oxidizing atmosphere, presents two characteristic regions of weight loss, indicating the formation of thermodynamically more stable oxidation products at approximately 500 °C, most likely products of carbonization and crosslinking: (i) during the initial stages of degradation (below 300 °C), oxidation, crosslinking and splitting of the chains may occur simultaneously, and in the case of oxidation and crosslinking, the mass loss is very small; and (ii) above 300 °C, oxidative degradation prevails, showing a sharp weight loss and the formation of aldehydes, ketones and carboxylic acids [29]. The oxidation of polyisoprene occurs between 300 and 400 °C. The small weight loss

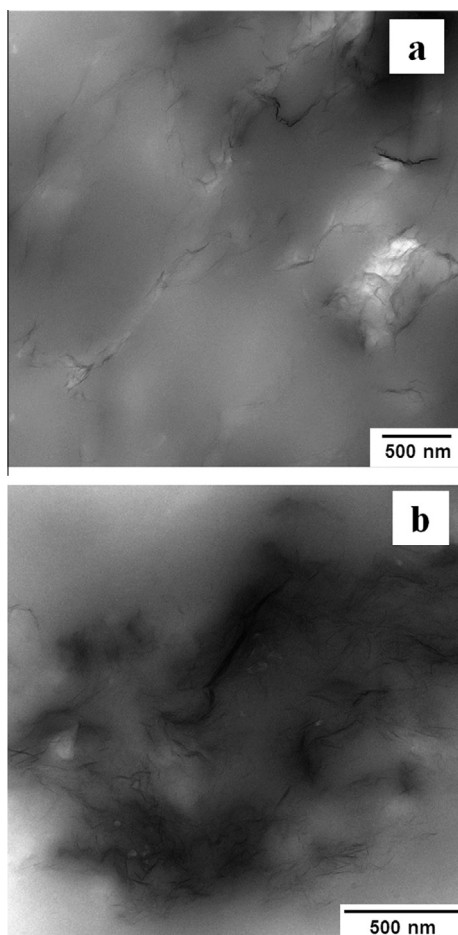


**Fig. 4** – TEM images of cryomicrotomed samples 2NRrGO (a) and 2NRGO (b) composites.

observed at approximately 430 °C is associated with the slow decomposition of the polymer chains and highly crosslinked polymeric residues. At temperatures higher than 500 °C, the polymer is degraded, and the final residues can be due compounds naturally present or derived from other substances found in natural rubber, like the phospholipids [30]. In the nanocomposites, the weight loss profiles have similar characteristics. Few differences were observed in the thermal properties between the natural rubber nanocomposites. In

nanocomposites with rGO (Fig. 7a), the degradation begins earlier than in the pure NR; this decrease in the degradation temperature is associated with the presence of the surfactant, cetyl ammonium bromide (CTAB), which decomposes in the range 260–310 °C [31]. The temperature at which the NRGO nanocomposite begins to degrade is quite similar to the unfilled polymer, indicating that the presence of GO does not affect the thermal stability of the rubber, an important factor in many applications involving natural rubber.

Fig. 8 shows the effect of the filler concentration on the electrical resistivity in the NR nanocomposites. The reported results are the average values obtained in duplicate in both directions on each side of the sample film. Networks are formed inside the composite from the addition of small quantities of graphene. The bidimensional character of graphene increases the probability of graphene-graphene contact, which explains the extremely low percolation threshold (between 0.1 and 0.5 wt%, very close to the value found by Zhan et al.) [32]. The addition of 2 wt% of graphene yielded a decrease in the electrical resistivity of 4 orders of magnitude ( $10^7$  to  $10^3 \Omega \text{ cm}$ ) compared to pure rubber. Kim et al. [20] show a reduction of 5 orders of magnitude ( $10^{11}$  to  $10^6 \Omega \text{ cm}$ ) in multi-layered graphene and styrene butadiene rubber composites using a heterocoagulation process. GO is an insulating material, and its insertion has little effect on the electrical properties of the material.

Fig. 9 shows the swelling curves in xylene (Fig. 9a and b), isopropanol (Fig. 9c and d) and water (Fig. 9e and f) for the neat NR and the nanocomposites with rGO and GO. In these curves, an inverse relationship between the percentage of absorption of the solvents and the amount of the nanostructures present in the material is observed, i.e., the more concentrated the nanocomposites are, the less solvent absorbed. All the nanocomposite samples absorb less solvent than the pure rubber, as shown in Table 2. The natural rubber shows an increase in mass of ~1900% for xylene, whereas the 2NRGO nanocomposite shows only 770%.

Fig. S3 shows images of squares pieces ( $1 \text{ cm} \times 1 \text{ cm} \times 0.5 \text{ mm}$ ) of natural rubber and 2NRrGO and 2NRGO nanocomposites at the beginning of the swelling experiment ( $t = 0$ ) and after 60 min of exposure to different solvents. After an hour of contact with the solvent, the polymer nanocomposites showed different degrees of swelling, which is much more evident in the case of xylene. For isopropyl alcohol and water,

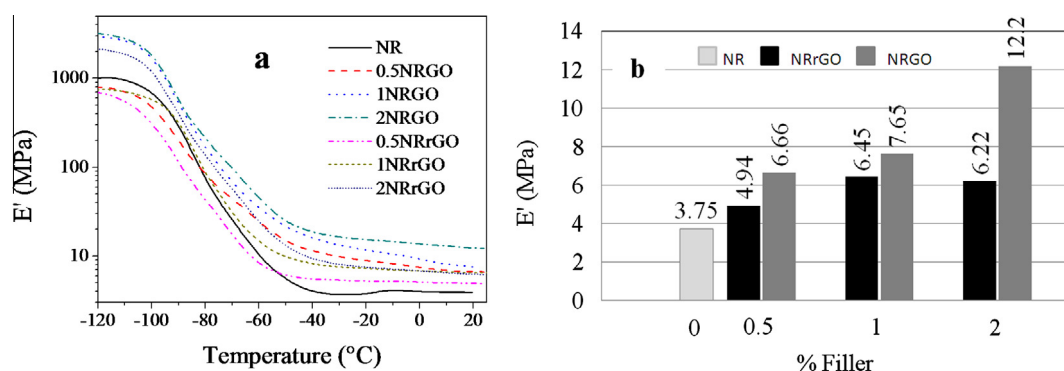


**Fig. 5** – (a) Storage modulus curves for NR and nanocomposites containing 0.5, 1 and 2 wt% of rGO and GO; (b) the storage modulus of the samples at 20 °C. (A colour version of this figure can be viewed online.)

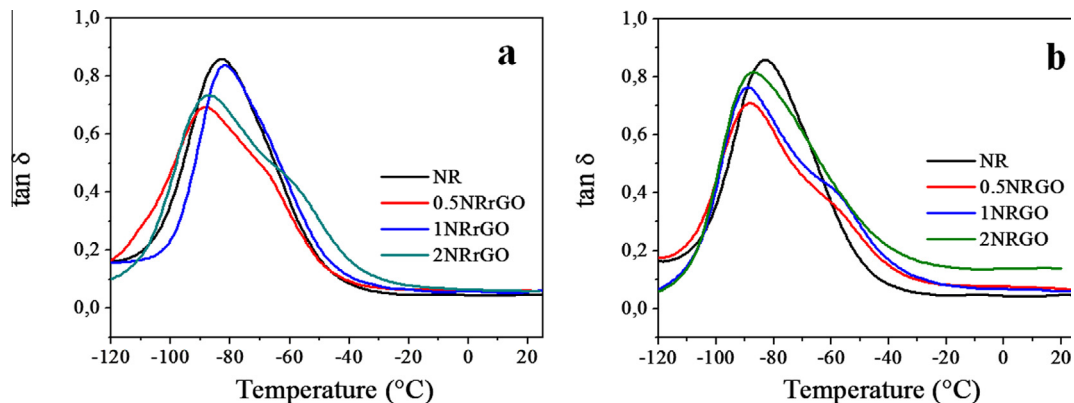


Fig. 6 – The  $\tan \delta$  peak versus temperature for NR and nanocomposite containing 0.5, 1 and 2 wt% of (a) rGO and (b) GO. (A colour version of this figure can be viewed online.)

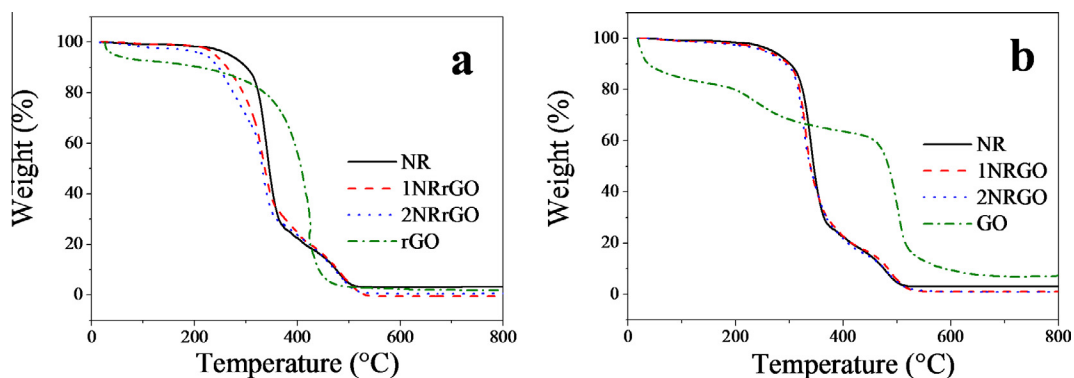


Fig. 7 – TGA curves of NR and (a) NRrGO and (b) NRGO nanocomposites, collected in a synthetic air atmosphere. (A colour version of this figure can be viewed online.)

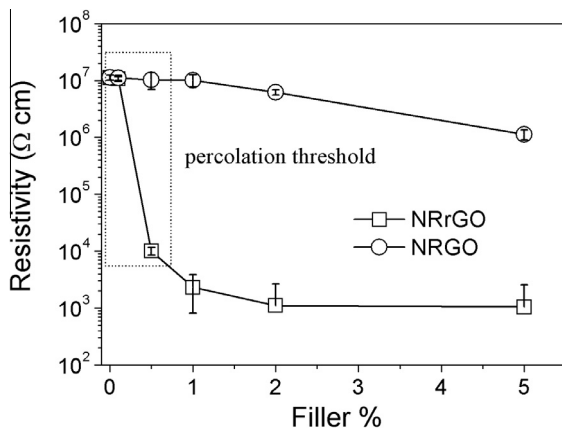


Fig. 8 – Resistivity as a function of filler loading for NR nanocomposites that contain rGO and GO.

the swelling is less than 10% of the total mass. The solvent resistance to xylene observed in this study was previously reported in the literature by incorporating other carbon nanostructures in matrices, such as natural rubber [33] and polyvinyl chloride [34]. This reduction in solvent absorption is more fully described by clays as the filling material in nanocomposites [24,35]. Because of such behavior, this type of nanocomposite is used in applications involving absorption resistance to solvents and gases [36], such as pipelines in

the petrochemical industry and food packaging, among others. A recent example is the work of Wu et al., [37] which showed a 48% reduction in air permeability for NR composites with only 0.3 wt% graphene.

The lower absorption of this type of nanocomposites is attributed to lamellar nanostructures, which act as a physical barrier that hinders the permeation of the solvent. In our case, in addition to acting as a physical barrier, this effect may also be due to networks of interconnected nanostructures that form a three-dimensional structure inside the composite, hindering movement of the polymer chains. For comparison, the mass gain in 60 min in nanocomposites containing 10 wt% clay [24] is ~750%, and it is 831% with 5 wt% carbon nanotubes [38], very close to the value of 770% observed for the 2NRGO sample and less than the value of 1800% of pure natural rubber.

For the other two solvents, which are much more polar than xylene and not considered good solvents for rubber, we also observed improvements in the solvent resistance. Depending on the nature of the solvent, the different degrees of resistance will be associated with the interaction between the polymer and the solvent (visible between NR and xylene), and for the first time, a direct relation with the polarity of the filler can also be observed. This result is clearly observed in the experiment with xylene, where the rGO composite swells less than the GO composite, while the behavior in water is the exactly the opposite. In isopropyl alcohol (intermediary

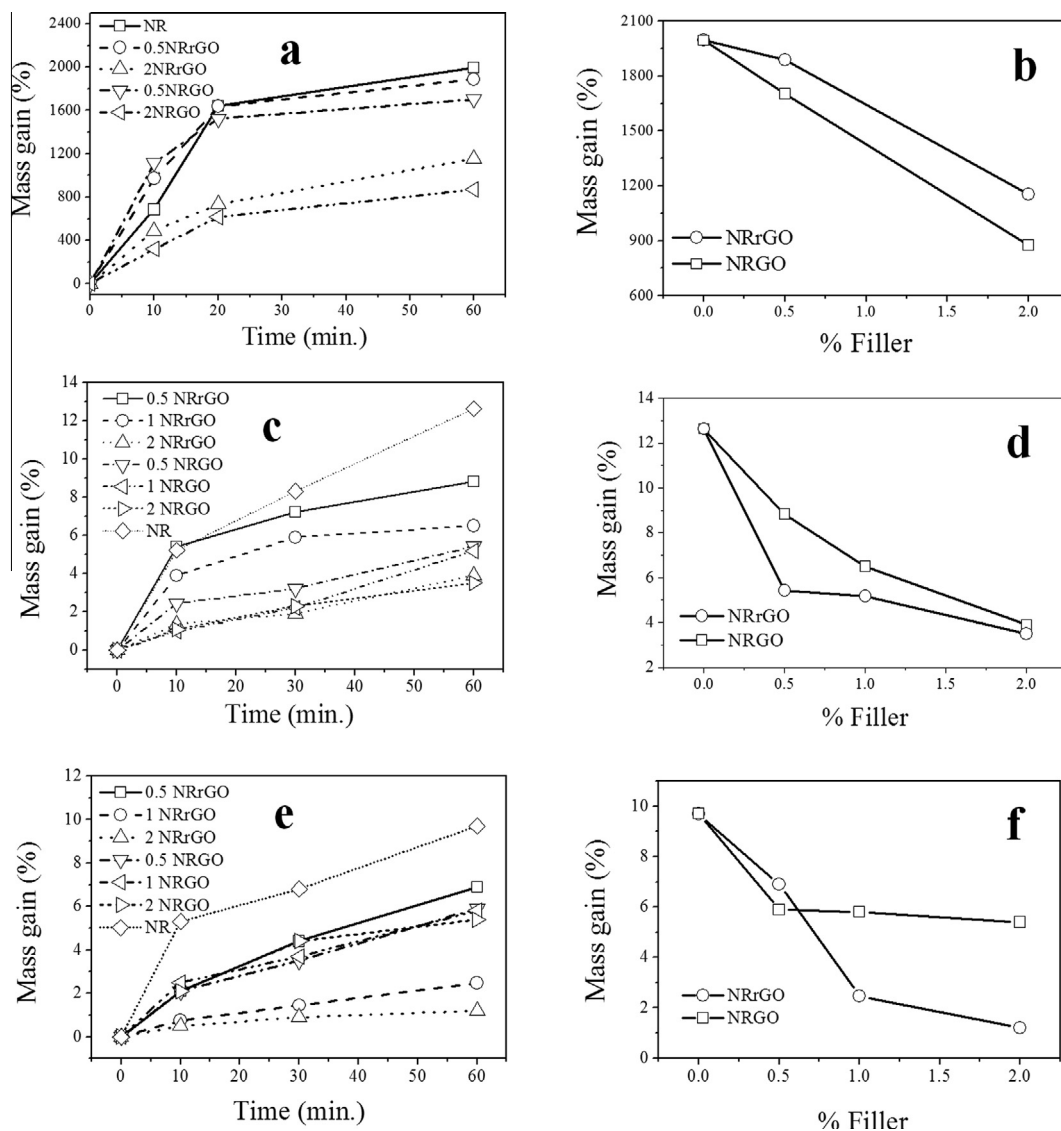


**Fig. 9** – Swelling curves for (a) xylene, (c) isopropyl alcohol and (e) water for samples of natural rubber nanocomposites and swelling of (b) xylene, (d) isopropyl alcohol and (f) water after 60 min as function of the amount of filler in the samples.

**Table 2** – Percentage of swelling of the samples after 1 h immersed in different solvents.

Sample	Xylene	Isopropyl alcohol	Water
NR	1895	12.6	9.7
0.5 NRrGO	1787	8.8	6.9
1 NRrGO	–	6.5	2.5
2 NRrGO	1054	3.9	1.2
0.5NRGO	1503	5.4	5.9
1 NRGO	–	5.2	5.8
2 NRGO	770	3.5	5.4

polarity) the differences between the fillers are minimal. This result is interesting because it is possible to modulate the chemical resistance of the material to different solvents or gases by altering the polarity of the filler and its concentration.

Finally, degradation tests were performed using nanocomposites containing 2 wt% of the nanostructures. Fig. 10a and b

show the physical aspect and percentage of material degradation over 12 months.

After 1 year, neat natural rubber (NR) showed a significant degradation of ~86%, whereas the 2NRrGO and 2NRGO nanocomposites showed degradations of 67% and 57%, respectively. The lower degradability versus time of the graphene-containing

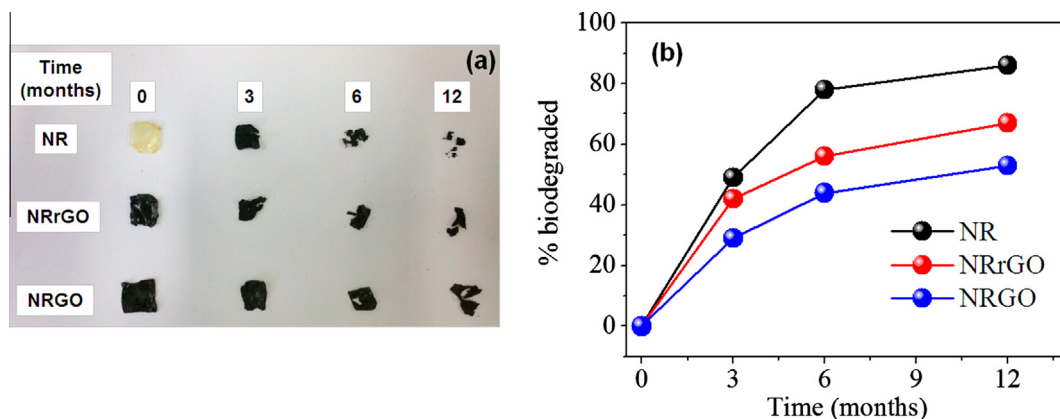


**Fig. 10 – (a) Physical aspect and (b) percentage of biodegradation of the material after 0, 3, 6 and 12 months in the soil. (A colour version of this figure can be viewed online.)**

species may be related to their known antibacterial properties [39]. This behavior may be interesting in biomedical applications and different applications of short duration, such as agriculture devices, packaging or other hygiene products.

Structural analysis using infrared spectroscopy and Raman spectroscopy showed the separation and oxidation of the polymer chain during all the process: infrared spectra (Supporting information, Fig. S4) shows clear signals of polymer degradation: (i) an increase in the band width intensity at approximately  $3340\text{ cm}^{-1}$ , indicating the formation of hydroxy compounds, such as alcohols and especially hydroperoxides; (ii) the convolution of the three bands approximately  $2900\text{ cm}^{-1}$  (stretching from  $\text{CH}_2$  groups); (iii) an increase in the intensity of the band in the  $1700\text{ cm}^{-1}$  region, indicating the formation of compounds contain carbonyl groups (aldehydes, ketones and acids); (iv) the band from unsaturated cis-1,4-bonds ( $720\text{ cm}^{-1}$ ) also decreases in intensity and disappears completely after 6 months of degradation, indicating an increase in crosslinking of the material.

From the Raman spectroscopy (Supporting information, Fig. S5), the disappearance of the band at  $1660\text{ cm}^{-1}$  (related to  $\text{C}=\text{C}$  stretching) and a significant decrease in the  $\text{CH}_x$  bands in the  $3200\text{--}2700\text{ cm}^{-1}$  region can be observed in all samples after 3 months in the soil, indicating degradation of the polymer chain. In the nanocomposites, there is a decrease in the G band at  $\sim 1580\text{ cm}^{-1}$  (the band that appears due to in-plane vibrations of  $\text{sp}^2$  carbon atoms) and an increase of D band ( $\sim 1330\text{ cm}^{-1}$ ) associated with the presence of  $\text{sp}^3$  carbons, heteroatoms and defects in the carbonic structure [40].

In general, it was possible to verify using vibrational techniques that the nanocomposites degrade similarly to pure NR. However, due to the presence of the nanostructures, the degradation process is slower.

#### 4. Conclusion

Different nanocomposite materials have been successfully prepared through the direct mixing of natural rubber latex and two different stable dispersions of rGO or GO in water. The natural rubber nanocomposites showed new chemical,

electrical and mechanical properties, dependent on the amount of filler, making them multifunctional materials and enabling a range of applications. Moreover, the biodegradability of these materials was confirmed, which, along with their “green” route of synthesis, make them environmentally friendly materials.

#### Acknowledgments

We gratefully acknowledge the financial support of CNPq, INCT of Carbon Nanomaterials (CNPq), NENNAM (Pronex, F. Araucária/CNPq), INCT of Complex Functional Materials (Inomat, CNPq and Fapesp) and LACTEC for the DMA measurements. CFM thanks CAPES for the fellowship.

#### Appendix A. Supplementary data

Supplementary data associated with this article can be found, in the online version, at <http://dx.doi.org/10.1016/j.carbon.2014.07.028>.

#### REFERENCES

- [1] Chiu CW, Huang TK, Wang YC, Alamani BG, Lin JJ. Intercalation strategies in clay/polymer hybrids. *Prog Polym Sci* 2014;39:443–85.
- [2] Huang JC. Carbon black filled conducting polymers and polymer blends. *Adv Polym Sci* 2002;21:299–313.
- [3] Al-Saleh MH, Sundararaj U. Review of the mechanical properties of carbon nanofiber/polymer composites. *Compos A* 2011;42:2126–42.
- [4] Rahmat M, Hubert P. Carbon nanotube–polymer interactions in nanocomposites: a review. *Compos Sci Technol* 2011;72:72–84.
- [5] Sham AYW, Notley SM. A review of fundamental properties and applications of polymer–graphene hybrid materials. *Soft Matter* 2013;9:6645–53.
- [6] Liu G, Neoh KG, Kang ET. Dispersible graphene oxide–polymer nanocomposites. *Polym-graphene Nanocompos* 2012;26:179.
- [7] Wang Y, Ameer GA, Sheppard BJ, Langer R. A tough biodegradable elastomer. *Nat Biotechnol* 2002;20:602–6.

- [8] Darder M, Aranda P, Ferrer ML, Gutiérrez MC, del Monte F, Ruiz-Hitzky E. Progress in bionanocomposite and bioinspired foams. *Adv Mater* 2011;23:5262–7.
- [9] Rippel MM, Leite CAP, Galembeck F. Elemental mapping in natural rubber latex films by electron energy loss spectroscopy associated with transmission electron microscopy. *Anal Chem* 2002;74:2541–6.
- [10] Sadasivuni KK, Ponnamma D, Thomas S, Grohens Y. Evolution from graphite to graphene elastomer composites. *Prog Polym Sci* 2013. <http://dx.doi.org/10.1016/j.progpolymsci.2013.08.003>.
- [11] Singh V, Joung D, Zhai L, Das S, Khondaker SI, Seal S. Graphene based materials: past, present and future. *Prog Mater Sci* 2011;56:1178–271.
- [12] Verdejo R, Bernal MM, Romasanta LJ, Lopez-Manchado MA. Graphene filled polymer nanocomposites. *J Mater Chem* 2011;21:3301–10.
- [13] Kim H, Abdala AA, Macosko CW. Graphene/polymer nanocomposites. *Macromolecules* 2010;43:6515–30.
- [14] Koning C, Grossiord N, Hermant MC. Polymer carbon nanotube composites: the polymer latex concept. Pan Stanford Pub; 2012.
- [15] Tkalya E, Ghislandi M, Alekseev A, Koning C, Loos J. Latex-based concept for the preparation of graphene-based polymer nanocomposites. *J Mater Chem* 2010;20:3035–3039.
- [16] Wu J, Xing W, Huang G, Li H, Tang M, Wu S, et al. *Polymer* 2013;54:3314–23.
- [17] Wu S, Tang Z, Guo B, Zhang L, Jia D. Vulcanization kinetics of graphene/natural rubber nanocomposites. *RSC Adv* 2013;3:443–85.
- [18] Domingues SH, Salvatierra RV, Oliveira MM, Zarbin AJG. Transparent and conductive thin films of graphene/polyaniline nanocomposites prepared through interfacial polymerization. *Chem Commun* 2011;47:2592–4.
- [19] Park S, Ruoff RS. Chemical methods for the production of graphenes. *Nat Nanotechnol* 2009;4:217–24.
- [20] Rippel MM, Lee LT, Leite CAP, Galembeck F. Skim and cream natural rubber particles: colloidal properties, coalescence and film formation. *J Colloid Interface Sci* 2003;268:330–40.
- [21] Kim J, Hong S, Park D, Shim S. Water-borne graphene-derived conductive SBR prepared by latex heterocoagulation. *Macromol Res* 2010;18:558–65.
- [22] Rippel MM, Leite CAP, Lee LT, Galembeck F. Formation of calcium crystallites in dry natural rubber particles. *J Colloid Interface Sci* 2005;288:449–56.
- [23] Potts JR, Shankar O, Du L, Ruoff RS. Processing–morphology–property relationships and composite theory analysis of reduced graphene oxide/natural rubber nanocomposites. *Macromolecules* 2012;45:6045–55.
- [24] Valadares LF, Leite CAP, Galembeck F. Preparation of natural rubber-montmorillonite nanocomposite in aqueous medium: evidence for polymer-platelet adhesion. *Polymer* 2006;47:672–8.
- [25] Cassu SN, Felisberti MI. Comportamento dinâmico-mecânico e relaxações em polímeros e blendas poliméricas. *Quim Nova* 2005;28:255–63.
- [26] Geethamma V, Kalaprasad G, Groeninckx G, Thomas S. Dynamic mechanical behavior of short coir fiber reinforced natural rubber composites. *Compos A* 2005;36:1499–506.
- [27] López-Manchado MA, Biagiotti J, Valentini L, Kenny JM. Dynamic mechanical and Raman spectroscopy studies on interaction between single-walled carbon nanotubes and natural rubber. *J Appl Polym Sci* 2004;92:3394–400.
- [28] Robertson CG, Rackaitis M. Further consideration of viscoelastic two glass transition behavior of nanoparticle-filled polymers. *Macromolecules* 2011;44:1177–81.
- [29] Li SD, Yu HP, Peng Z, Zhu CS, Li PS. Study on thermal degradation of sol and gel of natural rubber. *J Appl Polym Sci* 2000;75:1339–44.
- [30] Menon ARR, Pillai CKS, Nando GB. Thermal degradation characteristics of natural rubber vulcanizates modified with phosphorylated cashew nut shell liquid. *Polym Degrad Stab* 1996;52:265–71.
- [31] Uskoković V, Drogenik M, Ban I. The characterization of nanosized nickel-zinc ferrites synthesized within reverse micelles of CTAB/1-hexanol/water microemulsion. *J Magn Magn Mater* 2004;274:294–302.
- [32] Zhan Y, Lavorgna M, Buonocore G, Xia H. Enhancing electrical conductivity of rubber composites by constructing interconnected network of self-assembled graphene with latex mixing. *J Mater Chem* 2012;22:10464–8.
- [33] Bokobza L, Kolodziej M. On the use of carbon nanotubes as reinforcing fillers for elastomeric materials. *Polym Int* 2006;22:1090–8.
- [34] Broza G, Piszczek K, Schulte K, Sterzynski T. Nanocomposites of poly(vinyl chloride) with carbon nanotubes (CNT). *Compos Sci Technol* 2007;67:890–4.
- [35] Bragança FC, Valadares LF, Leite CAP, Galembeck F. Counterion effect on the morphological and mechanical properties of polymer–clay nanocomposites prepared in an aqueous medium. *Chem Mater* 2007;19:3334–42.
- [36] Scherillo G, Lavorgna M, Buonocore GG, Zhan YH, Xia HS, Mensitieri G, et al. Tailoring assembly of reduced graphene oxide nanosheets to control gas barrier properties of natural rubber nanocomposites. *ACS Appl Mater Interfaces* 2014;6:2230–4.
- [37] Wu J, Huang G, Li H, Wu S, Liu Y, Zheng J. Enhanced mechanical and gas barrier properties of rubber nanocomposites with surface functionalized graphene oxide at low content. *Polymer* 2013;54:1930–7.
- [38] Matos CF, Galembeck F, Zarbin AJG. Multifunctional materials based on iron/iron oxide-filled carbon nanotubes/natural rubber composites. *Carbon* 2012;50:4685–95.
- [39] Akhavan O, Ghaderi E. Toxicity of graphene and graphene oxide nanowalls against bacteria. *ACS Nano* 2010;4:5731–6.
- [40] Saito R, Hofmann M, Dresselhaus G, Jorio A, Dresselhaus MS. Raman spectroscopy of graphene and carbon nanotubes. *Adv Phys* 2011;60:413–550.